



## **Geophysical Research Letters**

## RESEARCH LETTER

10.1029/2020GL091413

#### **Key Points:**

- Continuous wavelet transforms reveal the dominant landforms defined by different wavelengths
- Synthetic drainages reveal that Cascadia is transitioning to a margin-parallel river system, supported by field observations of capture
- The Jaccard Similarity Index quantifies the scale-dependency of drainage network boundaries as topographic wavelength increases

#### **Supporting Information:**

· Supporting Information S1

#### Correspondence to:

W. Struble, wstruble@uoregon.edu

#### Citation:

Struble, W. T., Roering, J. J., Dorsey, R. J., & Bendick, R. (2021). Characteristic scales of drainage reorganization in Cascadia. *Geophysical Research Letters*, 48, e2020GL091413. https://doi.org/10.1029/2020GL091413

Received 27 OCT 2020 Accepted 19 DEC 2020

# **Characteristic Scales of Drainage Reorganization in Cascadia**

William T. Struble<sup>1</sup>, Joshua J. Roering<sup>1</sup>, Rebecca J. Dorsey<sup>1</sup>, and Rebecca Bendick<sup>2</sup>

<sup>1</sup>Department of Earth Sciences, University of Oregon, Eugene, OR, USA, <sup>2</sup>Department of Geosciences, University of Montana, Missoula, MT, USA

**Abstract** Variations in uplift, erosion, climate, and bedrock are commonly invoked as key controls on drainage basin morphology, yet the scale of landforms that define changes in regional drainage networks has not been addressed, limiting our ability to predict their planform evolution. Here we use two-dimensional (2D) continuous wavelet transforms of topography in Cascadia to highlight dominant topographic features at different scales. Surprisingly, our wavelet analysis shows that for wavelengths >30 km, the Cascadia Forearc Lowland (CFL) spans the entire margin. Separately, we compare observed catchment boundaries with synthetic boundaries generated on topography filtered with 2D Gaussian functions. We observe reorganization of synthetic drainage networks from an arc-to-coast drainage system into arc-spanning, margin-parallel river systems, akin to the modern Willamette River and coincident with the CFL. In concert with field observations of stream capture and Willamette Valley expansion, we propose that the Cascadia forearc is actively transitioning to a predominately margin-parallel river system.

**Plain Language Summary** River networks form as a result of the cumulative effects of bedrock uplift and erosional processes. Spatial variations in uplift, climate, and bedrock erodibility are typically considered to be the primary controls on the extent of drainage basins, yet the scale of landforms associated with drainage reorganization have not been systematically addressed. Here, we apply several filtering and topographic transformation techniques (two-dimensional continuous wavelet transforms and Gaussian filters) to extract landforms of variable scale and compare them to synthetic drainage networks in the Cascadia forearc. We observe that drainage networks mapped on filtered topography highlight growth of the Cascadia Forearc Lowland at scales >30 km. Integration of these "synthetic" drainage networks into a margin-parallel river system, similar to the modern Willamette Valley, supports field observations of stream capture and river network reorganization. We propose that these methods are useful for predicting future drainage configurations and isolating the relevant tectonic processes responsible for changing river networks.

#### 1. Introduction

The dynamic and tenuous nature of watershed boundaries, which define water resources, aquatic habitat, and the flux of sediment and organic materials, is readily apparent in landscapes that exhibit stream capture and drainage divide migration. The spatial extent and morphology of terrestrial river networks are dictated by the contribution of uplift acting over multiple spatiotemporal scales and the competing effects of erosion superimposed on variable bedrock lithologies (e.g., Forte et al., 2016; Gallen, 2018; Goren et al., 2014; Mitchell & Yanites, 2019; Whipple et al., 2017b). Where landscapes exist in a state of disequilibrium, such that drainage network morphology is not well adjusted to external drivers of uplift or erosion, channels respond by vertically incising or steepening (or aggrading and gentling; e.g., Kirby & Whipple, 2012), and drainage divides that separate adjacent catchments may horizontally migrate (e.g., Goren et al., 2014; Whipple et al., 2017b; Willett et al., 2014). As such, as uplift and erosion fluctuate over space and/or time, drainage basins continually evolve and morph from prior configurations in order to move toward "steady state" (Goren et al., 2014; Willett et al., 2014), though reorganization may continue long after significant uplift ceases (Beeson et al., 2017).

Prediction of the topographic scales responsible for setting drainage basin boundaries, and consequently the geophysical processes that drive drainage reorganization, has been an ongoing effort. River systems on Earth deviate markedly from predicted drainage pathways defined by long wavelength (>1,000 km)

© 2020. American Geophysical Union. All Rights Reserved.

STRUBLE ET AL. 1 of 11



topography owing to tectonic processes that act over shorter wavelengths and timescales, unlike on other planetary bodies such as Mars or Titan (Black et al., 2017). In terrestrial landscapes undergoing drainage reorganization, unstable divides appear to migrate toward long wavelength filtered (synthetic) topographic divides (Moodie et al., 2018; Wegmann et al., 2007). However, the precise scale of landforms that define the extent and stability of drainage basins remains unclear. Furthermore, while the direction of divide migration and in some cases the magnitude of disequilibrium can be predicted by local relief and river steepness (Forte & Whipple, 2018; Whipple et al., 2017b), hillcrest asymmetry (Mudd & Furbish, 2005), and the  $\chi$  metric, an integrated quantity of drainage area along a river profile (Perron & Royden, 2013; Willett et al., 2014), it is challenging to define the scale of processes responsible for drainage basin disequilibrium or diagnose why catchments exist in a state of dynamic adjustment (O'Hara et al., 2019; Whipple et al., 2017a; Yang et al., 2015).

Signal processing has proven successful in topographic and geophysical studies including drainage network and stream profile analysis (Black et al., 2017; Moodie et al., 2018; Roberts, 2019; Roberts et al., 2019; Wegmann et al., 2007), landform extraction and morphometrics (Doane et al., 2019; Lashermes et al., 2007; Perron et al., 2008; Sangireddy et al., 2017; Sare et al., 2019), and measurement of lithospheric thickness, mantle flow, and crustal strain rates (Audet, 2011, 2014; Bomberger et al., 2018; Davies et al., 2019; Turcotte et al., 2002). Here, we demonstrate that two-dimensional (2D) continuous wavelet transforms (CWTs) of topography highlight the scale of landforms defined by local structural, lithologic, and base level controls as well as regional landforms defined by subduction and mantle flow; many of these landforms do not correspond with mapped drainage divides. In addition, we separately establish the scale-dependency of drainage basins by mapping synthetic drainage networks on topography Gaussian filtered to progressively longer wavelengths. Where the elevation and location of topographic highs differ between Gaussian-filtered digital elevation models, major river divides appear to migrate. We isolate the scale-dependency of drainage basins by quantifying the similarity between synthetic drainage basin boundaries and those of the actual landscape by using the Jaccard Similarity Index (JSI), a statistic of the degree of overlap (i.e., similarity) between the sample sets (Jaccard, 1900).

We focus on the central and southern Cascadia forearc, including the Klamath, Rogue, Umpqua, and Willamette Rivers (Figure 1, S1), where drainage reorganization is a common and ongoing process. Multiple large discrete stream captures have been mapped at the crest of the Oregon Coast Range (OCR) along the western margin of the Willamette Valley (WV) (Baldwin & Howell, 1949; Chylek, 2002; Moeller, 1990; Niem, 1976) and in the Umpqua and Rogue River catchments (Figures S1, S2, and S3), where rivers that used to flow directly from the Cascades to the Pacific Ocean (arc-to-coast) were diverted into margin-parallel catchments such as the Willamette River. The driver of these reorganization events, including the role of uplift in the OCR, remains ambiguous; potential controls on river network changes include crustal faults bounding alluviated valleys that contribute to basin subsidence and geomorphic adjustment (Blakely et al., 2000; von Dassow, 2018; Wells et al., 2017, 1998; Yeats et al., 1996) as well as deeper subduction processes (e.g., Becker et al., 2014; Blakely et al., 2005; Delph et al., 2018; Ramachandran et al., 2006).

#### 2. Methods

We utilized 3-arc second (90 m) Shuttle Radar Topography Mission (SRTM) digital elevation models (DEMs), a sufficient resolution to ensure that major rivers route correctly and low-relief drainage divides are accurately resolved. To visualize the pattern of dominant landforms over various wavelengths <200 km, we applied CWTs to a DEM spanning the entire Cascadia margin. This analysis enables us to identify the wavelengths at which particular physiographic features become readily apparent. Separately, in order to identify the scales at which discrete changes in catchment boundaries and substantial modifications to the regional drainage network configuration occur, we filtered (i.e., smoothed), topography over progressively longer wavelengths using Gaussian filtering and mapped synthetic drainage networks and corresponding drainage divides. We then quantified the similarity of these synthetic drainage basins to those generated with the unfiltered DEM to establish the scale-dependency of the drainage network and constrain the topographic wavelengths that are responsible for drainage basin evolution.

STRUBLE ET AL. 2 of 11

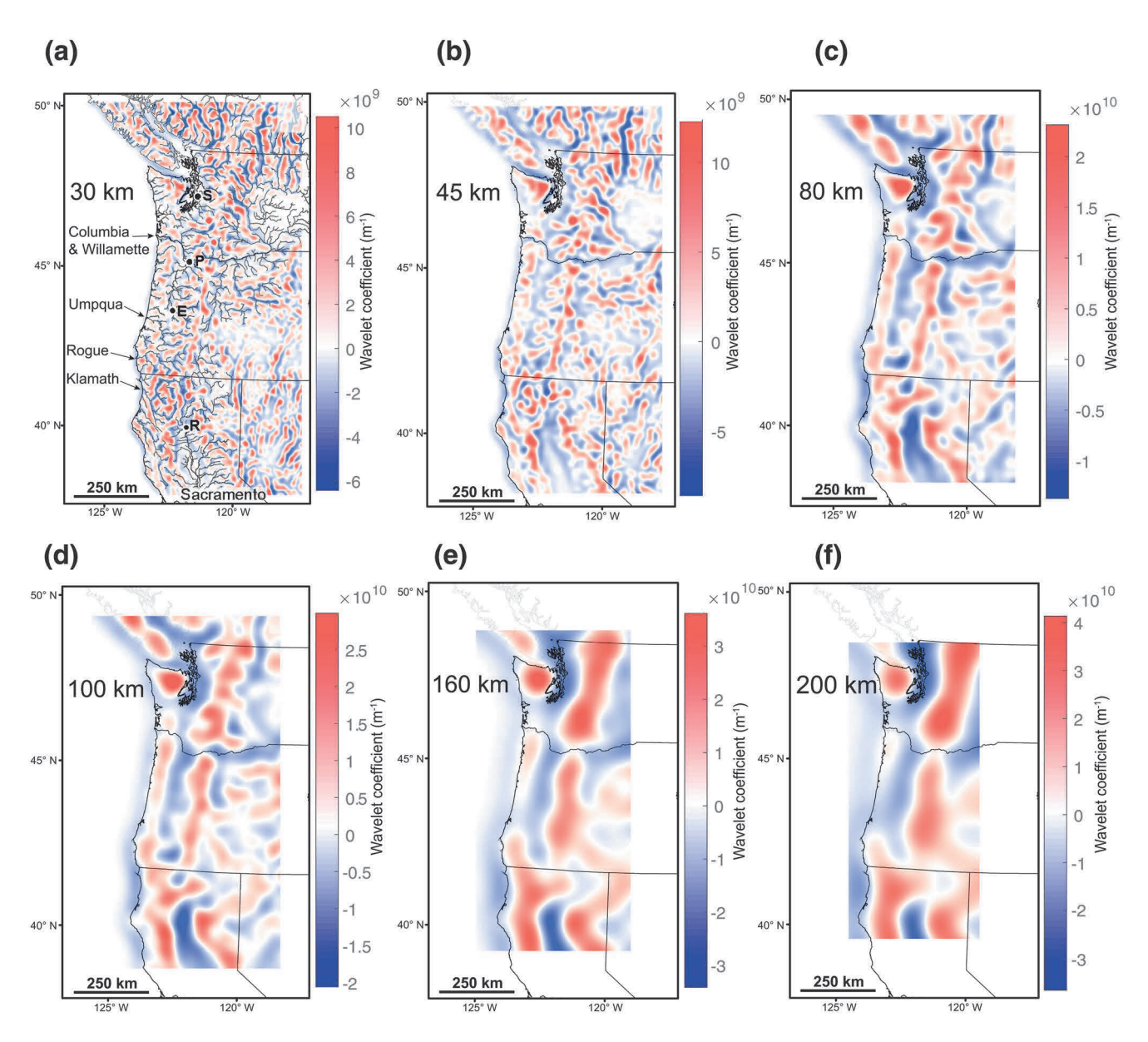


Figure 1. Two dimensional (2D) Continuous wavelet transform of topography reveals convex (red) and concave (blue) regions corresponding to the specified wavelength. Dominant landforms observed: (a) 30 km wavelength: Hillslopes and valleys, potentially corresponding with lithologic contrasts and shallow crustal faults (Basin and Range). Cascades volcanoes apparent. Gray lines are major rivers, labeled at outlet. Great Basin rivers omitted. See Figure S1 for all rivers and landforms labeled and wind gap locations. (b) 45 km: Broader landforms reveal influence of regional tectonics. Willamette Valley (WV) displays connectivity with neighboring drainage basins. (c) 80 km: WV and other forearc lowlands consolidating. (d–e) 100 km-160 km: Cascadia Forearc Lowland clearly apparent. (f) 200 km: Olympic and Klamath Mountains and Cascades Arc persist. Growing white space corresponds with clipped wavelet edge effects, a width approximately four times the wavelet scale. S: Seattle, P: Portland, (e) Eugene, R: Redding.

## 2.1. Continuous Wavelet Transforms: Ricker Wavelet

We applied a 2D CWT to the SRTM topographic data using the Ricker (Mexican Hat) wavelet. The Ricker wavelet is often used in topographic analyses (Booth et al., 2009; Malamud & Turcotte, 2001; Turcotte et al., 2002) and depicts the Laplacian of topography (Lashermes et al., 2007; Torrence & Compo, 1998), revealing concave and convex regions (Figure 1). These mapped concave and convex regions, or landforms, reveal dominant features as defined by the wavelet scale. Hence, unlike a Gaussian filter, which removes high-wavenumber information, or a band-pass filter, which isolates a range of wavelengths, the CWT allows for visualization of topography corresponding to a specific wavelength. High magnitude wavelet coefficients

STRUBLE ET AL. 3 of 11



denote where the wavelength of topographic curvature corresponds well to the specified wavelet scale. Thus, a large positive (negative) wavelet coefficient at a particular wavelength indicates that topography is strongly convex (concave) at that wavelength.

The CWT using the Ricker wavelet is computationally efficient, has few edge effects, and does not assume stationarity (constant mean, variance) of topographic data (Torrence & Compo, 1998). The generalized 2D CWT, with a wavelet scale parameter s, elevation z, and location (u,v) is given as

$$C(s,u,v) = \frac{1}{s} \int_{-\infty}^{\infty} \int_{-\infty}^{\infty} z(x,y) \psi\left(\frac{x-u}{s}, \frac{y-v}{s}\right) dxdy$$
 (1)

where  $\psi$  is a wavelet family and C is the resultant wavelet coefficient. Hence, the 2D CWT is a convolution of z and  $\psi$ ,

$$C(s,u,v) = \frac{1}{s}z(x,y) * \psi\left(\frac{x-u}{s}, \frac{y-v}{s}\right)$$
 (2)

A wavelet with a large wavelet scale, s, produces a broad  $\psi$  that reveals long wavelength elements in z, while small values of s produce a small  $\psi$ , which in turn defines the finer features in z. In other words, a large (small) wavelet scale extracts long (short) wavelength features in topography.

We defined the relevant scale, *s*, of the Ricker wavelet using its Fourier wavelength, which is the inverse of its band-pass frequency (Foufoula-Georgiou & Kumar, 1994; Mallat, 1999). The Fourier wavelength for a derivative of a Gaussian is defined as,

$$\lambda = \frac{2\pi s}{\sqrt{m + \frac{1}{2}}}\tag{3}$$

where m is the mth derivative of a Gaussian (Torrence & Compo, 1998). Since the Ricker wavelet is the negative second derivative of a Gaussian, m=2. Hence, larger wavelet scales, s, correspond to larger topographic wavelengths,  $\lambda$ . Reorganizing Equation 3, we solved for s for each topographic wavelength of interest, in this case wavelengths from 5 km to 200 km in increments of 5 km. For each wavelength, we then used Equation 2 to convolve topography with the 2D Ricker wavelet, given as,

$$\psi_R(x,y) = (2 - x^2 - y^2) \exp\left[-\frac{1}{2}(x^2 + y^2)\right]$$
 (4)

The resultant wavelet coefficients output from Equation 2 signify concave and convex topographic landforms corresponding to the input wavelet scale (Figure 1).

## 2.2. Gaussian Filter and Jaccard Similarity Index

To characterize the scale-dependence of forearc drainage networks, we filtered (i.e., smoothed) the raw SRTM topographic data using a 2D Gaussian function in 5 km increments up to 200 km. We used the resulting filtered DEMs to map synthetic drainage networks and drainage divides. Thus, the resultant drainage networks are those that would form without the influence of topography that corresponds to a wavenumber higher than the filter scale. For this analysis, an inverse wavelet transform of coefficients from the CWT could be used to reconstruct topography for particular wavelengths (Figure 1). Instead, we choose to use a 2D Gaussian filter which has the advantage of preserving the longest wavelength landforms as these are primarily responsible for setting the form of river longitudinal profiles (Roberts, 2019; Roberts et al., 2019). The 2D Gaussian function is defined as,

$$\psi_G(x,y) = \frac{1}{2\pi s^2} \exp\left[-\frac{(u-x)^2 + (v-y)^2}{2s^2}\right]$$
 (5)

STRUBLE ET AL. 4 of 11

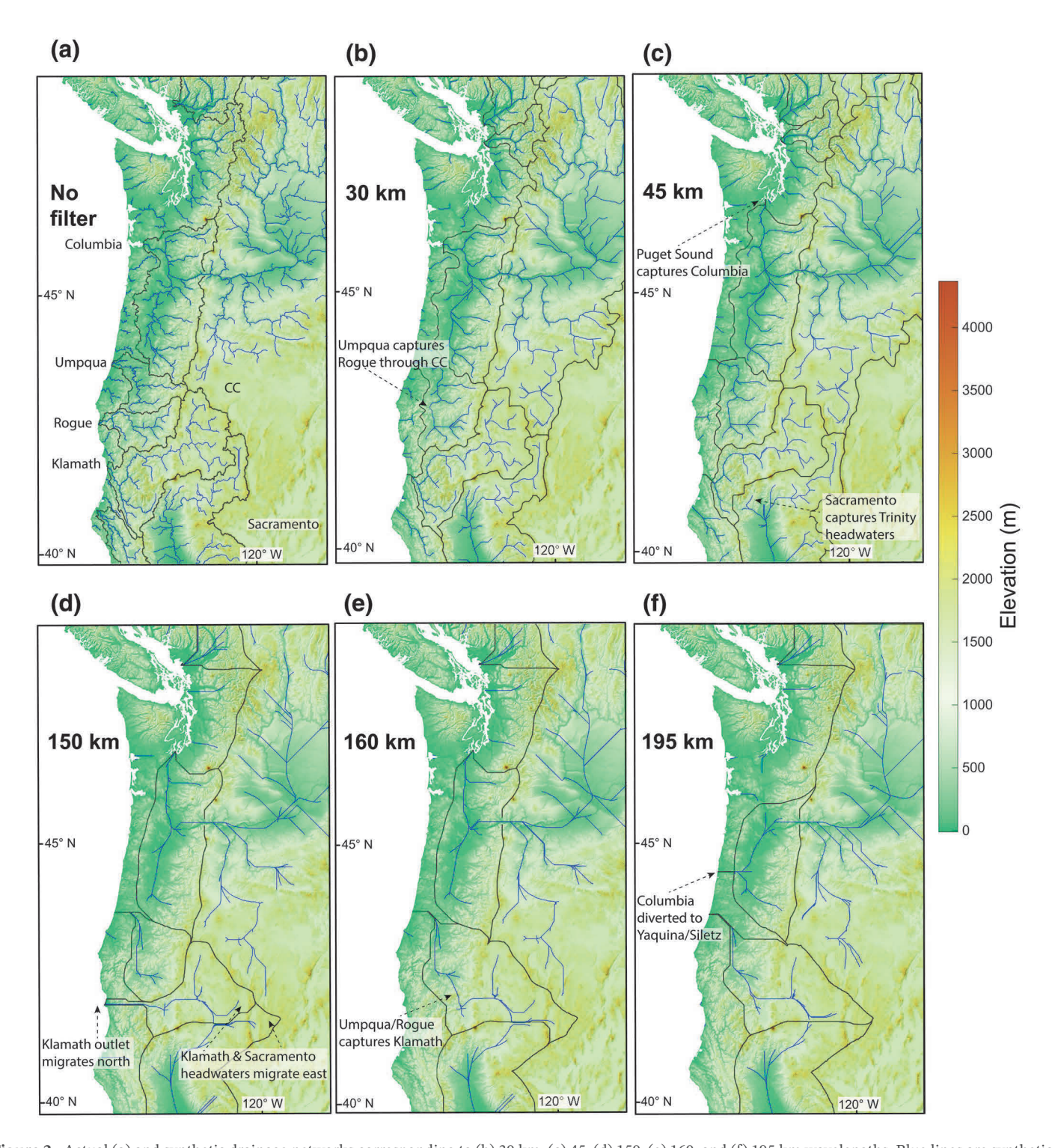


Figure 2. Actual (a) and synthetic drainage networks corresponding to (b) 30 km, (c) 45, (d) 150, (e) 160, and (f) 195 km wavelengths. Blue lines are synthetic drainage networks, and gray lines are synthetic drainage divides corresponding to major forearc drainage basins. Each panel highlights discrete changes to drainage basin extent, defined by drops in JSI (Figure 3). See text for description of each major change. For visual clarity, mapped topography in all panels is unfiltered (Figure S5 for filtered). Linear channels correspond with filled sinks (prevalent in the upper Columbia Basin). These sinks do not affect our results in the forearc. We plot the drainage divide at the crest of the Cascades for Willamette-draining channels (i.e., no upper Columbia). CC: Cow Creek.

STRUBLE ET AL. 5 of 11



For each topographic wavelength (5 km–200 km), we solved for the appropriate scale, s, of the filter using the Fourier wavelength of a Gaussian function, defined in Equation 3. For a 2D Gaussian function, m=0 (Torrence & Compo, 1998). We filtered the raw topography DEM with the appropriately scaled Gaussian function by convolution of  $\psi_G$  with topography, z, as denoted in Equation 2, thus producing a smoothed DEM (Figure S5; Sangireddy et al., 2017).

We produced synthetic drainage networks that correspond to each Gaussian filtered DEM by routing flow over each filtered DEM with the D8 flow routing algorithm in MATLAB using TopoToolbox (Schwanghart & Scherler, 2014), and we mapped the resulting synthetic drainage divides for forearc catchments with trunk channels that drain to sea level (Figures 2, S2, and S5). These synthetic stream networks are those that would form without any influence of landforms smaller than the scale of the Gaussian filter wavelength. We clipped the Columbia River at the crest of the Cascades in the Columbia River Gorge to limit the drainage divides to those that flow into the WV.

In order to pinpoint the wavelengths at which discrete changes to drainage basins occur, we calculated the similarity between each synthetic and unfiltered drainage basin using the Boolean JSI (Jaccard, 1900; Levandowsky & Winter 1971), defined as:

$$JSI = \frac{\left| B_o \cap B_f \right|}{\left| B_o \right| + \left| B_f \right| + \left| B_o \cap B_f \right|} \tag{6}$$

where  $B_0$  is the original, or unfiltered, drainage basin and  $B_f$  is the synthetic drainage basin. When JSI = 1,  $B_0$  and  $B_f$  are identical when JSI = 0, the drainage basins have no overlap. Thus, fluctuations in JSI correspond to changes in drainage basin extent in the Gaussian filtered DEMs (Figure 3). Specifically, gradual and abrupt drops in JSI at particular wavelengths correspond to synthetic divide migration and stream capture, respectively, between drainage basins in Gaussian filtered and unfiltered DEMs (Figure 3). JSI has been used previously to quantify the divide migration between timesteps in a landscape evolution model (O'Hara et al., 2019) and how well modeled lava flows predict real flows (Richardson & Karlstrom, 2019). Our use of JSI here, however, is the first to quantify the scale-dependency of drainage network boundaries as a function of topographic wavelength. Finally, since Gaussian filtering tends to "smear" topography, thus shifting the coastline and decreasing JSI, we clipped both filtered and unfiltered drainage basin outlets at sea level defined in unfiltered topography.

## 3. Results

## 3.1. 2D CWT Reveals Cascadia Forearc Landforms

The 2D CWT of topography for each applied wavelet scale reveals concave and convex landforms corresponding to particular wavelengths. In other words, high-magnitude wavelet coefficients for a particular scale denote landforms well characterized by that wavelength. Specifically, at small wavelengths (<30 km), we observe that high magnitude wavelet coefficients highlight and correspond well with hillslopes and valleys, volcanoes in the Cascades, and shallow crustal structures, such as normal fault-bounded mountain ranges in the Basin and Range Province (Figure 1a). As wavelength increases, regional landforms that span multiple river catchments become more apparent (Figure 1b). Specifically, for wavelengths at which the contribution of subduction zone deformation is dominant (~80 km-160 km; Becker et al., 2014; Bomberger et al., 2018 and references therein), the coastal ranges and Cascades arc continuously traverse the entire length of the subduction zone. We similarly observe persistent lengthening of the WV as it merges with nearby depositional basins in the southern and northern extents of the margin (Figure 1c), including the Puget Lowland. We note, however, that connectivity exists between arc-parallel lowland terrain at wavelengths as small as 45 km (Figure 1b). At wavelengths of 100 km and higher, this Cascadia Forearc Lowland extends along the entire margin of the subduction zone, from the Strait of Georgia in the north to Mount Shasta in the south (Figures 1d-1f). While the coastal ranges become less prominent at wavelengths >150 km, the high-elevation Olympic and Klamath Mountains remain pronounced, potentially a reflection of rapid uplift rates associated with localized mantle upwelling (Balco et al., 2013; Bodmer et al., 2019; Kelsey et al., 1994).

STRUBLE ET AL. 6 of 11

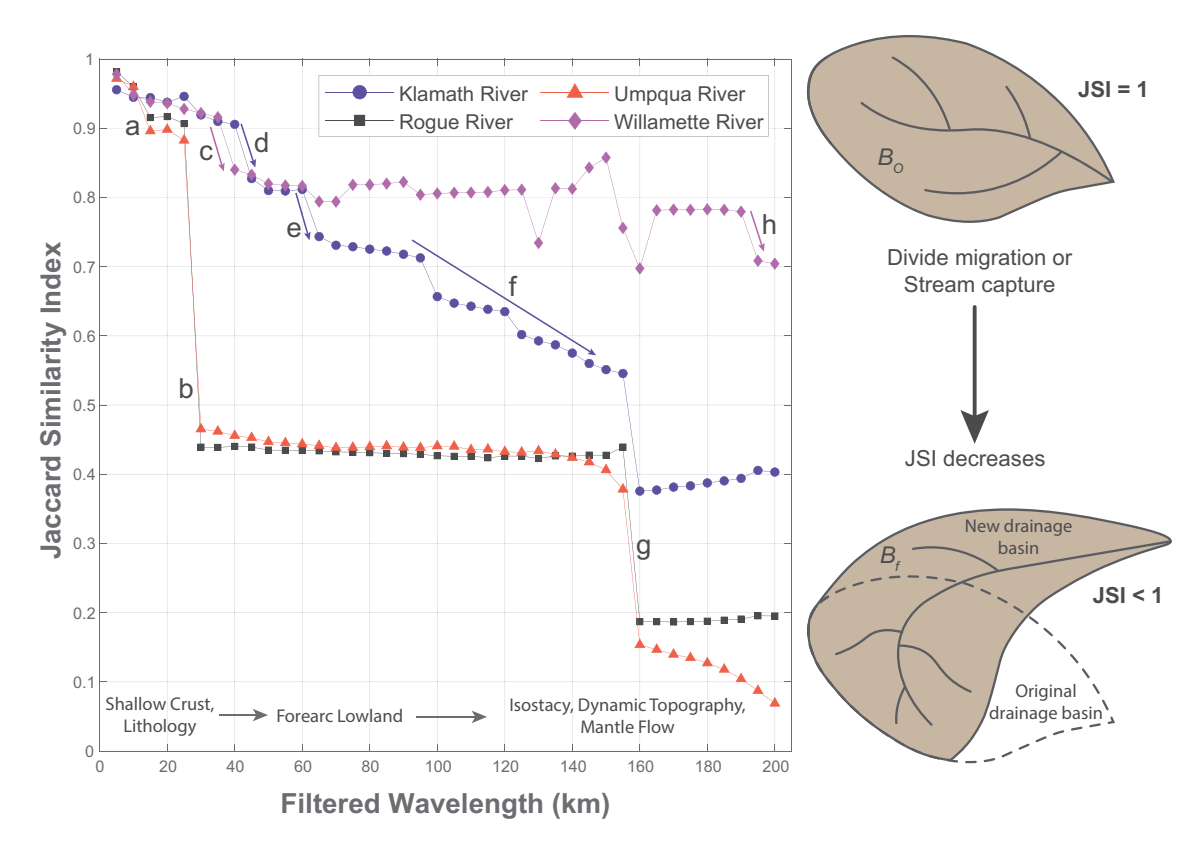


Figure 3. Jaccard Similarity Index (JSI) quantifies scale-dependence of drainage basins. High JSI indicates little change between synthetic and unfiltered catchments. Low JSI indicates greater change due to mobile divides and captures. Drops in JSI include: (a) 15 km wavelength: Synthetic capture of Cow Creek by Rogue River. (b) 30 km: Umpqua River captures the Rogue River through Cow Creek, indicating reverse in capture direction. (c) 40 km: Willamette River diverted into Puget Sound. (d) 45 km: Sacramento River captures Trinity River headwaters (Klamath River tributary). (e) 65 km: trunk channel of Trinity River drains directly to sea level. (f) ~90 km-155 km: Klamath River outlet migrates northward. (g) 160 km: Klamath River diverted into merged Umpqua/Rogue system. (h) 190 km: Willamette River diverted across Marys/Yaquina drainage divide. Oscillation in JSI for Willamette River between 130 km and 160 km due to Columbia River outlet alternating between Chehalis River and Puget Sound. Oscillation an artifact introduced from Pleistocene glaciation due to clipping outlets at sea level.

Finally, the longest analyzed wavelengths ( $\sim$ 160 km–200 km) correspond to integrated whole-lithosphere effects such as gravitational potential flows and coupling with mantle flow, most apparent in the Cascades and High Lava Plains (Figures 1e and 1f; Becker et al., 2014; Faccenna & Becker, 2020). We acknowledge, however, that the limited size of our study area and the clipping of edge effects (e.g., Figure 1f) lend caution to our analysis of these longest wavelength landforms.

## 3.2. Synthetic Drainage Networks Reveal the Future of Cascadia Forearc Drainages

Stream captures are common along the western margin of the WV and Cascadia Forearc Lowland, where rivers that previously flowed from the arc to the coast were diverted into the Willamette River (Figures S1 and S2; Baldwin & Howell, 1949; Chylek, 2002; Moeller, 1990; Niem, 1976). The extension of the WV in 2D CWT topography beyond its mapped drainage divides and the observation that stream capture is an ongoing process that appears to be migrating south through time (Baldwin & Howell, 1949; Chylek, 2002), encourages an examination of how the drainage network is adjusting to long wavelength landforms and variations in uplift rate between the OCR and the Cascadia Forearc Lowland.

To constrain the scale dependence of the Cascadia drainage network, we calculated JSI for the Willamette, Umpqua, Rogue, and Klamath Rivers, as they remain coherent drainage basins across a wide range of wavelengths. JSI values for the Rogue and the Umpqua Rivers gradually decrease as Gaussian filter wavelength increases, up to  $\sim$ 15 km, at which point the synthetic divide between the Umpqua and Rogue Rivers shifts

STRUBLE ET AL. 7 of 11



northward as the synthetic Rogue River captures Cow Creek (Figures S1 and S2), the southernmost tributary of the Umpqua River that was recently captured from the Coquille River (Figure S3). Synthetic capture of Cow Creek by the Rogue River is partially explained by the lack of adjustment of Cow Creek to base level lowering imposed by the Umpqua basin–knickpoints resulting from recent capture from the Coquille River have yet to migrate to the low-relief headwaters captured by the synthetic Rogue River (Figure S3). This low-relief reach of Cow Creek appears in filtered topography as a broad, poorly integrated surface primed for capture. At a wavelength of 30 km, however, the polarity of synthetic divide migration reverses, and the synthetic Umpqua River captures the Rogue River through Cow Creek (Figures 2 and S2), resulting in an abrupt drop in JSI for both the Rogue and Umpqua Rivers (Figure 3). Synthetic capture of the Rogue River by the Umpqua River reflects progressive and continuing growth of the Umpqua drainage basin and suggests that faster uplift in the southern OCR and Klamath Mountains may drive the Rogue River to seek a new route to base level (Balco et al., 2013; Bodmer et al., 2019; von Dassow, 2018; Kelsey et al., 1994).

In the Klamath River catchment, we observe multiple abrupt drops in JSI superimposed on a gradual overall decrease (Figure 3). Abrupt drops in JSI at wavelengths <160 km correspond to synthetic drainage basin augmentation in the Klamath River headwaters in the Basin and Range Province and High Lava Plains east of the Cascades and loss of southern tributaries in the Klamath Mountains. The main stem of the Klamath River has kept pace with high-uplift rates in the Klamath Mountains, as indicated by its well-entrenched valley system through the range. Entrenchment of the Klamath River is reflected by the remarkable stability of the main stem of the river through a wide range of wavelengths, although the synthetic outlet of the river migrates northward at longer (100 km–155 km) wavelengths (Figures 2 and 3). At a wavelength of 160 km, the synthetic Klamath River is diverted northward into the merged Umpqua-Rogue system (Figures 2 and 3). In addition, southern tributaries of the Klamath River, including the Trinity River, which may be experiencing higher uplift as the Mendocino Triple Junction passes (Balco et al., 2013; Bodmer et al., 2019; Furlong & Govers, 1999; Kelsey et al., 1994; Lock et al., 2018), are diverted at moderate wavelengths (40 km–45 km; Figures 2 and 3).

The Willamette River experiences the smallest overall decrease in JSI (Figure 3), reflecting concordance between the modern WV and the Cascadia Forearc Lowland that we observe in wavelet-transformed topography (Figures 1 and S1). Regions of simulated divide migration and stream capture support geologic evidence for progressive growth and southward migration of the WV that accentuates the forearc lowland (Figures 2 and S2). Between 40 km and 45 km wavelengths, the Columbia River is diverted into the Puget Lowland over the low divide between the Chehalis and Cowlitz Rivers, which is composed of glacial outwash that has inundated the forearc (Figure 2). Despite the significant depth of structural basins in the Puget Lowland (e.g., Ramachandran et al., 2006), the role of tectonics and basin subsidence in driving this capture event may be somewhat modulated by Plio-Pleistocene glaciation in the Puget Lowland, though Columbia River sediments have been mapped at the mouth of the Chehalis River (Walsh et al., 1987). Other regions of simulated transience and capture in the northern WV are concentrated along drainage divides with the Nehalem and Nestucca Rivers and are supported by Paleoroutes of the Columbia River (Figure S2), indicated by emplacement patterns of the Columbia River Basalts (Beeson et al., 1989; Reidel & Tolan, 2013). In the southwestern WV, we observe mobility of simulated drainage divides with west-draining OCR rivers (Figure S2), where multiple discrete captures along the divides with the Siuslaw, Alsea, Yaquina, and Siletz Rivers have been observed (Figure 1; Baldwin & Howell, 1949; Chylek, 2002; Moeller, 1990; Niem, 1976). Given these captures have already occurred, offset between the synthetic and modern divides is minimal.

## 4. Discussion and Conclusions

Application of 2D CWTs and Gaussian filters to topography informs the scale and distribution of catchment-defining landforms, which then dictate drainage divide migration over a broad suite of wavelengths. Notably, in Ricker wavelet-transformed topography, the concave Cascadia Forearc Lowland exhibits some connectivity at wavelengths >30 km (Figures 1a–1c), and it clearly extends along the entire subduction zone at wavelengths >100 km (Figures 1d–1f). In turn, synthetic drainage networks mapped on Gaussian filtered topography illuminate the scale dependency of drainage basins in the Cascadia forearc (Figure 3) and highlight the influence of hillslope-valley coupling, lithology, and shallow crustal faults at short wavelengths

STRUBLE ET AL. 8 of 11



(<30 km), regional tectonic deformation at intermediate wavelengths (30 km-160 km), and lithospheric mechanics or mantle processes at long wavelengths (160 km-200 km).

The locations of simulated capture points identified in our analysis coincide with independent geologic evidence for shifting drainages, allowing us to hindcast past captures and predict future captures of coast-draining rivers in southern Cascadia. When coupled with field observations of stream capture and growth of margin-parallel rivers in the forearc (Figures 2, S3, and S4; Baldwin & Howell, 1949; Chylek, 2002; Moeller, 1990; Niem, 1976), the simulated diversion of arc-to-coast rivers at wavelengths >30 km suggests that Gaussian filtered topography is an effective predictor of future divide transience and stream capture between major river catchments. Geologic variability in lithology and structure modulate and control drainage basin morphology and contribute to drainage reorganization on short temporal and spatial scales (Forte et al., 2016; Gallen, 2018), including intracatchment reorganization. Nonetheless, long-wavelength topography better predicts future drainage configurations (Campbell, 1896; Moodie et al., 2018; Wegmann et al., 2007), as it is more persistent than transitory lithologic and structural heterogeneities. Persistence of long-wavelength topographic divides provides a prolonged, exogenic boundary condition that directs the flow of rivers and alters the geometry of drainage networks (Faccenna et al., 2019; Moodie et al., 2018).

Our results suggest that southern Cascadia arc-to-coast draining rivers (Umpqua, Rogue, Klamath) are evolving into a configuration more evocative of the WV. Observed WV captures and predicted future growth of margin-parallel rivers is likely a result of differential uplift along the margin, continued OCR uplift that outpaces river incision, and/or active subsidence within the forearc topographic low, though the relative importance of these options is unclear. We suggest, however, that observed growth of the WV in concert with the formation of structural basins (e.g., Blakely et al., 2000; McPhee et al., 2014) implicates crustal subsidence as an important boundary condition for setting drainage network geometry and driving forearc drainage reorganization. The spatial variability in uplift rates that would be implied by the transition of the Cascadia forearc to a margin-parallel river system may be due to recent reorganization of oceanic plates and subduction (Bassett & Watts, 2015; Bodmer et al., 2015; Calvert et al., 2011; Hawley & Allen, 2019); mantle wedge serpentinization, corner flow, and high rates of slab sinking driving forearc subsidence and/or OCR uplift (Audet et al., 2010; Becker et al., 2014; Blakely et al., 2005; Brocher et al., 2003; Delph et al., 2018; Hyndman & Peacock, 2003; Johnson & Tebo, 2018; Ramachandran et al., 2006); clockwise rotation and crustal faulting of the forearc forcing basin formation (Blakely et al., 2000; Wells & McCaffrey, 2013; Wells et al., 2017, 1998); or some combination thereof. Isolating the effect of these mechanisms on topography, while beyond the scope of this work, will elucidate the role of variable-scale tectonic processes on setting drainage basin morphology, as well as clarify active processes driving relief formation in forearcs.

Utilization of 2D CWTs and Gaussian filters represents a promising paradigm for interpreting drainage network disequilibrium and predicting future pathways of reorganization as well as investigating the characteristic wavelength of tectonic and surface processes that define and dictate river network extent and morphology. Wavelet- and Gaussian-transformed topography may be exploited to inform fish genetics and paleogeographic reconstructions, sediment provenance, and landscape evolution models and may provide linkages between surface processes and mantle and crustal dynamics measured using seismic tomography and geodesy. Finally, future studies are needed to address how river discharge and sediment supply interact with variable-wavelength topography, and whether Gaussian filtered synthetic drainage networks correspond with specific timescales of landscape transience and adjustment.

## **Data Availability Statement**

All SRTM topographic data are available for download from OpenTopography (https://portal.opentopography.org/raster?opentopoID=OTSRTM.082015.4326.1) or in MATLAB through TopoToolbox (https://topotoolbox.wordpress.com).

#### References

Audet, P. (2011). Directional wavelet analysis on the sphere: Application to gravity and topography of the terrestrial planets. *Journal of Geophysical Research*, 116(E1), E01003. https://doi.org/10.1029/2010JE003710

#### Acknowledgments

The author thanks N. Finnegan, D. O'Hara, J. O'Connor, R. Wells, L. Karlstrom, N. Klema, S. LaHusen, and T. Doane for helpful discussions. The authors are particularly grateful to Adam Booth, who provided several helpful conversations about wavelets. and whose Automated Landslide Mapping toolkit (ALMtools) served as the initial framework for the wavelet analysis done here (http://web.pdx. edu/~boothad/tools.html). A. Moodie and an anonymous reviewer provided thoughtful comments that greatly improved the quality of this paper. W. T. Struble was supported by a Lokey Doctoral Fellowship through the University

STRUBLE ET AL. 9 of 11



- Audet, P. (2014). Toward mapping the effective elastic thickness of planetary lithospheres from a spherical wavelet analysis of gravity and topography. *Physics of the Earth and Planetary Interiors*, 226, 48–82. https://doi.org/10.1016/j.pepi.2013.09.011
- Audet, P., Bostock, M. G., Boyarko, D. C., Brudzinski, M. R., & Allen, R. M. (2010). Slab morphology in the Cascadia fore arc and its relation to episodic tremor and slip. *Journal of Geophysical Research*, 115, B00A16. https://doi.org/10.1029/2008JB006053
- Balco, G., Finnegan, N., Gendaszek, A., Stone, J. O., & Thompson, N. (2013). Erosional response to northward-propagating crustal thickening in the coastal ranges of the US Pacific Northwest. *American Journal of Science*, 313(8), 790–806.
- Baldwin, E. M., & Howell, P. W. (1949). The Long Tom, a Former Tributary of the Siuslaw River. Northwest Science, 23, 112-124.
- Bassett, D., & Watts, A. B. (2015). Gravity anomalies, crustal structure, and seismicity at subduction zones: 2. Interrelationships between forearc structure and seismogenic behavior. Geochemistry, Geophysics, Geosystems, 16(5), 1541–1576. https://doi.org/10.1002/2014GC005685
- Becker, T. W., Faccenna, C., Humphreys, E. D., Lowry, A. R., & Miller, M. S. (2014). Static and dynamic support of western United States topography. Earth and Planetary Science Letters, 402, 234–246. https://doi.org/10.1016/j.epsl.2013.10.012
- Beeson, H. W., McCoy, S. W., & Keen-Zebert, A. (2017). Geometric disequilibrium of river basins produces long-lived transient landscapes. Earth and Planetary Science Letters, 475, 34–43. https://doi.org/10.1016/j.epsl.2017.07.010
- Beeson, M. H., Tolan, T. L., & Anderson, J. L. (1989). The Columbia River Basalt Group in Western Oregon; Geologic structures and other factors that controlled flow emplacement patterns. *Geological Society of America*, Special Paper 239, .223.
- Black, B. A., Perron, J. T., Hemingway, D., Bailey, E., Nimmo, F., & Zebker, H. (2017). Global drainage patterns and the origins of topographic relief on Earth, Mars, and Titan. Science, 356(6339), 727–731. https://doi.org/10.1126/science.aag0171
- Blakely, R. J., Wells, R. E., Tolan, T. L., Beeson, M. H., Trehu, A. M., & Liberty, L. M. (2000). New aeromagnetic data reveal large strike-slip (?) faults in the northern Willamette Valley, Oregon. *Geological Society of America Bulletin*, 9.
- Blakely, R. J., Brocher, T. M., & Wells, R. E. (2005). Subduction-zone magnetic anomalies and implications for hydrated forearc mantle. Geology, 33(6), 445–448. https://doi.org/10.1130/G21447.1
- Bodmer, M., Toomey, D. R., Roering, J. J., & Karlstrom, L. (2019). Asthenospheric buoyancy and the origin of high-relief topography along the Cascadia forearc. *Earth and Planetary Science Letters*, 115965. https://doi.org/10.1016/j.epsl.2019.115965
- Bodmer, M., Toomey, D. R., Hooft, E. E., Nábělek, J., & Braunmiller, J. (2015). Seismic anisotropy beneath the Juan de Fuca plate system: Evidence for heterogeneous mantle flow. *Geology*, 1, G37181. https://doi.org/10.1130/G37181.1
- Bomberger, C., Bendick, R., Flesch, L., & Ehlers, T. A. (2018). Spatial Scales in topography and strain rate magnitude in the western United States. *Journal of Geophysical Research: Solid Earth*, 123(7), 6086–6097. https://doi.org/10.1029/2018JB016135
- Booth, A. M., Roering, J. J., & Perron, J. T. (2009). Automated landslide mapping using spectral analysis and high-resolution topographic data: Puget Sound lowlands, Washington, and Portland Hills, Oregon. *Geomorphology*, 109(3–4), 132–147. https://doi.org/10.1016/j.geomorph.2009.02.027
- Brocher, T. M., Parsons, T., Trehu, A. M., Snelson, C. M., & Fisher, M. A. (2003). Seismic evidence for widespread serpentinized forearc upper mantle along the Cascadia margin. *Geology*, 31(3), 267–270.
- Calvert, A. J., Preston, L. A., & Farahbod, A. M. (2011). Sedimentary underplating at the Cascadia mantle-wedge corner revealed by seismic imaging. *Nature Geoscience*, 4(8), 545–548. https://doi.org/10.1038/ngeo1195
- Campbell, M. R. (1896). Drainage Modifications and Their Interpretation. The Journal of Geology, 4(5), 567-581.
- Chylek, S. J. (2002). GIS Analysis of Quaternary Stream Capture in the Eastern Coast Range, Western Oregon (Undergraduate Honors Thesis). University of Oregon.
- Davies, D. R., Valentine, A. P., Kramer, S. C., Rawlinson, N., Hoggard, M. J., Eakin, C. M., & Wilson, C. R. (2019). Earth's multi-scale topographic response to global mantle flow. *Nature Geoscience*, 12(10), 845–850. https://doi.org/10.1038/s41561-019-0441-4
- Delph, J. R., Levander, A., & Niu, F. (2018). Fluid controls on the heterogeneous seismic characteristics of the Cascadia margin. Geophysical Research Letters, 45(20). https://doi.org/10.1029/2018GL079518
- Doane, T. H., Roth, D. L., Roering, J. J., & Furbish, D. J. (2019). Compression and decay of hillslope topographic variance in Fourier wavenumber domain. *Journal of Geophysical Research: Earth Surface*. https://doi.org/10.1029/2018JF004724
- Faccenna, C., Glišović, P., Forte, A., Becker, T. W., Garzanti, E., Sembroni, A., & Gvirtzman, Z. (2019). Role of dynamic topography in sustaining the Nile River over 30 million years. *Nature Geoscience*. https://doi.org/10.1038/s41561-019-0472-x
- Faccenna, C., & Becker, T. W. (2020). Topographic expressions of mantle dynamics in the Mediterranean. *Earth-Science Reviews*, 209, 103327. https://doi.org/10.1016/j.earscirev.2020.103327
- Forte, A. M., & Whipple, K. X. (2018). Criteria and tools for determining drainage divide stability. Earth and Planetary Science Letters, 493, 102–117. https://doi.org/10.1016/j.epsl.2018.04.026
- Forte, A. M., Yanites, B. J., & Whipple, K. X. (2016). Complexities of landscape evolution during incision through layered stratigraphy with contrasts in rock strength. *Earth Surface Processes and Landforms*. 41. 1736–1757.
- Foufoula-Georgiou, E., & Kumar, P. (1994). Wavelet Analysis and its Applications (Vol. 4, p. 372). New York, NY: Academic Press. https://doi.org/10.1016/B978-0-08-052087-2.50007-4
- Furlong, K. P., & Govers, R. (1999). Ephemeral crustal thickening at a triple junction: The Mendocino crustal conveyor. *Geology*, 27(2), 127–130. https://doi.org/10.1130/0091-7613(1999)027<0127:ECTAAT>2.3.CO;2
- Gallen, S. F. (2018). Lithologic controls on landscape dynamics and aquatic species evolution in post-orogenic mountains. Earth and Planetary Science Letters, 493, 150–160. https://doi.org/10.1016/j.epsl.2018.04.029
- Goren, L., Willett, S. D., Herman, F., & Braun, J. (2014). Coupled numerical-analytical approach to landscape evolution modeling. *Earth Surface Processes and Landforms*, 39(4), 522–545. https://doi.org/10.1002/esp.3514
- Hawley, W. B., & Allen, R. M. (2019). The fragmented death of the farallon plate. Geophysical Research Letters, 2019GL083437. https://doi.org/10.1029/2019GL083437
- Hyndman, R. D., & Peacock, S. M. (2003). Serpentinization of the forearc mantle. Earth and Planetary Science Letters, 212(3-4), 417-432. https://doi.org/10.1016/S0012-821X(03)00263-2
- Jaccard, P. (1900). Étude comparative de la distribution florale dans une portion des Alpes et des Jura. Bulletin de La Societe Vaudoise Des Sciences Naturelles, 37(142), 547–579. https://doi.org/10.5169/seals-266450
- Johnson, K. M., & Tebo, D. (2018). Capturing 50 Years of Postseismic mantle flow at Nankai subduction zone. Journal of Geophysical Research: Solid Earth, 123(11)–10091–10106. https://doi.org/10.1029/2018JB016345
- Kelsey, H. M., Engebretson, D. C., Mitchell, C. E., & Ticknor, R. L. (1994). Topographic form of the Coast Ranges of the Cascadia Margin in relation to coastal uplift rates and plate subduction. *Journal of Geophysical Research*, 99(B6), 12245–12255.
- Kirby, E., & Whipple, K. X. (2012). Expression of active tectonics in erosional landscapes. *Journal of Structural Geology*, 44, 54–75. https://doi.org/10.1016/j.jsg.2012.07.009

STRUBLE ET AL. 10 of 11



- Lashermes, B., Foufoula-Georgiou, E., & Dietrich, W. E. (2007). Channel network extraction from high resolution topography using wavelets. *Geophysical Research Letters*, 34(23). https://doi.org/10.1029/2007GL031140
- Levandowsky, M., & Winter, D. (1971). Distance between sets. Nature, 234, 34-35.
- Lock, J., Kelsey, H., Furlong, K., & Woolace, A. (2018). Late Neogene and quaternary landscape evolution of the Northern California coast ranges: Evidence for Mendocino triple junction tectonics. Geological Society of America Bulletin, 15.
- Malamud, B. D., & Turcotte, D. L. (2001). Wavelet analyses of Mars polar topography. *Journal of Geophysical Research: Planets*, 106(E8), 17497–17504. https://doi.org/10.1029/2000JE001333
- Mallat, S. (1999). A wavelet tour of signal processing (2nd Ed.). San Diego, CA: Elsevier.
- McPhee, D. K., Langenheim, V. E., Wells, R. E., & Blakely, R. J. (2014). Tectonic evolution of the Tualatin basin, northwest Oregon, as revealed by inversion of gravity data. *Geosphere*, 10(2), 264–275. https://doi.org/10.1130/GES00929.1
- Mitchell, N. A., & Yanites, B. J. (2019). Spatially variable increase in rock uplift in the northern U.S. Cordillera recorded in the distribution of river knickpoints and incision depths. *Journal of Geophysical Research Earth Surface*, 124, 1238–1260. https://doi.org/10.1029/2018JF004880
- Moeller, B. (1990). Stream capture in the central Oregon coast range and its relationship to tectonic and structural geology (Masters Thesis). Eugene, OR: University of Oregon.
- Moodie, A. J., Pazzaglia, F. J., & Berti, C. (2018). Exogenic forcing and autogenic processes on continental divide location and mobility. Basin Research, 30(2), 344–369. https://doi.org/10.1111/bre.12256
- Mudd, S. M., & Furbish, D. J. (2005). Lateral migration of hillcrests in response to channel incision in soil-mantled landscapes. *Journal of Geophysical Research*, 110(F4). https://doi.org/10.1029/2005JF000313
- Niem, W. A. (1976). Drainage basin morphology in the central coast range of Oregon (Masters Thesis). Oregon State University.
- O'Hara, D., Karlstrom, L., & Roering, J. J. (2019). Distributed landscape response to localized uplift and the fragility of steady states. *Earth and Planetary Science Letters*, 506, 243–254. https://doi.org/10.1016/j.epsl.2018.11.006
- Perron, J. T., Kirchner, J. W., & Dietrich, W. E. (2008). Spectral signatures of characteristic spatial scales and nonfractal structure in land-scapes. *Journal of Geophysical Research*, 113(F4). https://doi.org/10.1029/2007JF000866
- Perron, J. T., & Royden, L. (2013). An integral approach to bedrock river profile analysis. Earth Surface Processes and Landforms, 38(6), 570–576. https://doi.org/10.1002/esp.3302
- Ramachandran, K., Hyndman, R. D., & Brocher, T. M. (2006). Regional P wave velocity structure of the Northern Cascadia Subduction Zone. *Journal of Geophysical Research*, 111(B12). https://doi.org/10.1029/2005JB004108
- Reidel, S. P., & Tolan, T. L. (2013). The late Cenozoic evolution of the Columbia River system in the Columbia River flood basalt province. In:
  Geological Society of America special papers (Vol. 497, 201–230). Geological Society of America. https://doi.org/10.1130/2013.2497(08)
- Richardson, P., & Karlstrom, L. (2019). The multi-scale influence of topography on lava flow morphology. *Bulletin of Volcanology*, 81(4), 21. https://doi.org/10.1007/s00445-019-1278-9
- Roberts, G. G. (2019). Scales of similarity and disparity between drainage networks. Geophysical Research Letters. https://doi. org/10.1029/2019GL082446
- Roberts, G. G., White, N., & Lodhia, B. H. (2019). The generation and scaling of longitudinal river profiles. *Journal of Geophysical Research:* Earth Surface, 124(1), 137–153. https://doi.org/10.1029/2018JF004796
- Sangireddy, H., Stark, C. P., & Passalacqua, P. (2017). Multiresolution analysis of characteristic length scales with high-resolution topographic data. *Journal of Geophysical Research: Earth Surface*, 122(7), 1296–1324. https://doi.org/10.1002/2015JF003788
- Sare, R., Hilley, G. E., & DeLong, S. B. (2019). Regional-scale detection of fault scarps and other tectonic landforms: Examples from Northern California. *Journal of Geophysical Research: Solid Earth*, 124(1), 1016–1035. https://doi.org/10.1029/2018JB016886
- Schwanghart, W., & Scherler, D. (2014). Short Communication: TopoToolbox 2 MATLAB-based software for topographic analysis and modeling in Earth surface sciences. Earth Surface Dynamics, 2(1), 1–7. https://doi.org/10.5194/esurf-2-1-2014
- Torrence, C., & Compo, G. P. (1998). A practical guide to wavelet analysis. Bulletin of the American Meteorological Society, 79(1), 18.
- Turcotte, D. L., Shcherbakov, R., Malamud, B. D., & Kucinskas, A. B. (2002). Is the Martian crust also the Martian elastic lithosphere?. Journal of Geophysical Research, 107(E11), 1–1 1–20. https://doi.org/10.1029/2001JE001594
- von Dassow, W. (2018). Geomorphic evidence for differential rock uplift across the southern Cascadia forearc (Masters Thesis). Oregon State University.
- Walsh, T. J., Korosec, M. A., Phillips, W. M., Logan, R. L., & Schasse, H. W. (1987). Geologic map of Washington-Southwest quadrant.
- Wegmann, K. W., Zurek, B. D., Regalla, C. A., Bilardello, D., Wollenberg, J. L., Kopczynski, S. E., et al. (2007). Position of the Snake River watershed divide as an indicator of geodynamic processes in the greater Yellowstone region, western North America. *Geosphere*, 3(4), 272–281. https://doi.org/10.1130/GES00083.1
- Wells, R. E., Blakely, R. J., Wech, A. G., McCrory, P. A., & Michael, A. (2017). Cascadia subduction tremor muted by crustal faults. *Geology*, 45(6), 515–518. https://doi.org/10.1130/G38835.1
- Wells, R. E., & McCaffrey, R. (2013). Steady rotation of the Cascade arc. Geology, 41(9), 1027–1030. https://doi.org/10.1130/G34514.1
- Wells, R. E., Weaver, C. S., & Blakely, R. J. (1998). Fore-arc migration in Cascadia and its neotectonic significance. *Geology*, 26(8), 759–762. Whipple, K. X., DiBiase, R. A., Ouimet, W. B., & Forte, A. M. (2017a). Preservation or piracy: Diagnosing low-relief, high-elevation surface formation mechanisms. *Geology*, 45(1), 91–94. https://doi.org/10.1130/G38490.1
- Whipple, K. X., Forte, A. M., DiBiase, R. A., Gasparini, N. M., & Ouimet, W. B. (2017b). Timescales of landscape response to divide migration and drainage capture: Implications for the role of divide mobility in landscape evolution: Landscape response to divide mobility. Journal of Geophysical Research: Earth Surface. https://doi.org/10.1002/2016JF003973
- Willett, S. D., McCoy, S. W., Perron, J. T., Goren, L., & Chen, C.-Y. (2014). Dynamic reorganization of river basins. *Science*, 343(6175), 1248765–1248765. https://doi.org/10.1126/science.1248765
- Yang, R., Willett, S. D., & Goren, L. (2015). In situ low-relief landscape formation as a result of river network disruption. *Nature*, 520(7548), 526–529. https://doi.org/10.1038/nature14354
- Yeats, R. S., Graven, E. P., Werner, K. S., Goldfinger, C., & Popowski, T. A. (1996). Tectonics of the Willamette Valley, Oregon (Vol. 1). US Government Printing Office.

STRUBLE ET AL. 11 of 11